ChemPubSoc Europe

DOI: 10.1002/cphc.201700743

CHEMPHYSCHEM Articles

VIP *Very Important Paper*

Role of the Chalcogen (S, Se, Te) in the Oxidation Mechanism of the Glutathione Peroxidase Active Site

Marco Bortoli[+],[a] Mauro Torsello[+],[b] F. Matthias Bickelhaupt,*[c, d] and Laura Orian*[a]

The oxidation by H_2O_2 of the human phospholipid hydroperoxide glutathione peroxidase (GPx4), used as a model peroxidase selenoenzyme, as well as that of its cysteine (Cys) and tellurocysteine (Tec) mutants, was investigated in silico through a combined classic and quantum mechanics approach to assess the role of the different chalcogens. To perform this analysis, new parameters for selenocysteine (Sec) and tellurocysteine (Tec) were accurately derived for the AMBER ff14SB force field. The oxidation represents the initial step of the antioxidant activity of GPx, which catalyzes the reduction of H_2O_2 and organic hydroperoxides by glutathione (GSH). A mechanism involving a charge-separation intermediate is feasible for the Cys and Sec enzymes, leading from the initial thiol/selenol form to sulfenic/selenenic acid, whereas for the Tec mutant a direct oxidation pathway is proposed. Activation strain analyses, performed for Cys-GPx and Sec-GPx, provided insight into the rate-accelerating effect of selenium as compared to sulfur and the role of specific amino acids other than Cys/Sec that are typically conserved in the catalytic pocket.

1. Introduction

There is currently an intense debate on the biological role of selenium, which so far has been discovered in 25 human proteins in the form of selenocysteine (Sec), and most of these human proteins are key enzymes involved in balancing oxidative stress.[1–3] The limited presence of selenium is certainly a result of evolutionary pressure, and its involvement in a small number of reactions suggests some advantage over sulfur, which in theory could imitate the physiological role of selenium. Unluckily, after exactly 200 years since its discovery, the understanding of the function of selenium in the living cell is still fragmentary. From a chemical perspective, the Sec residue exhibits different characteristics than cysteine (Cys): a lower pK_a (5.2 vs. 8.3)[4] and superior leaving group and electron-acceptor abilities,[5] all of which do not straightforwardly explain why in some cases nature has chosen selenium rather than sulfur.[6] In addition, in some complex eukaryotes, Sec can be replaced by Cys without significant loss in activity,[7] and this suggests that to shed more light on the role of selenium in biological systems, a deeper and more systematic investigation is required on the chemical, biochemical, and biological activity of natural and artificial model systems.

A pivotal role in modulating the cellular peroxide tone in mammals is played by glutathione peroxidase (GPx). This class of ubiquitous enzymes catalyzes the reduction of H_2O_2 and, in general, organic hydroperoxides by using reduced glutathione (GSH),[8] which thus keeps the level of cellular oxidative stress at bay. In addition, the role of glutathione peroxidases extends beyond mere antioxidant defense to redox-regulated peroxide sensors and signal transducers.[9] The GPx enzymatic mechanism involves three steps (Scheme 1): the oxidation of selenol **E** to selenenic acid **F**, accompanied by the reduction of the hydroperoxide; 2 equivalents of GSH are consumed in the two subsequent reductive steps to form selenenyl sulfide intermediate **G** and oxidized glutathione (i.e. GSSG) with regeneration of the initial selenol.[10,11]

Four types of selenium-containing GPx exist. The first to be described was GPx1 (also called cytosolic or cellular GPx); it is tetrameric and can interact with a wide variety of organic peroxides, but it is highly specific for glutathione as a reducing substrate.[12]

Like GPx1, GPx2 (also called gastrointestinal GPx) is tetrameric and has over 65% chain identity with GPx1 and similar substrate specificity.[13] GPx3 is a glycoprotein found mainly in human plasma. Its role as an extracellular antioxidant has been questioned due to the low concentration of GSH in plasma, though it seems it can function in conjunction with thioredox-

[a] *M. Bortoli,[+] Prof. Dr. L. Orian*
Dipartimento di Scienze Chimiche
Università degli Studi di Padova
Via Marzolo 1 35129 Padova (Italy)
E-mail: laura.orian@unipd.it

[b] *Dr. M. Torsello[+]*
Present address:
via Trieste 38, 25121 Brescia (Italy)

[c] *Prof. Dr. F. M. Bickelhaupt*
Department of Theoretical Chemistry
and Amsterdam Center for Multiscale Modeling (ACMM)
Vrije Universiteit Amsterdam
De Boelelaan 1083, 1081 HV Amsterdam (The Netherlands)
E-mail: f.m.bickelhaupt@vu.nl

[d] *Prof. Dr. F. M. Bickelhaupt*
Institute for Molecules and Materials (IMM)
Radboud University
Heyendaalseweg 135, 6525 J Nijmegen (The Netherlands)

[+] *These authors contributed equally to this work.*

Supporting Information and the ORCID identification number(s) for the author(s) of this article can be found under: https://doi.org/10.1002/cphc.201700743.

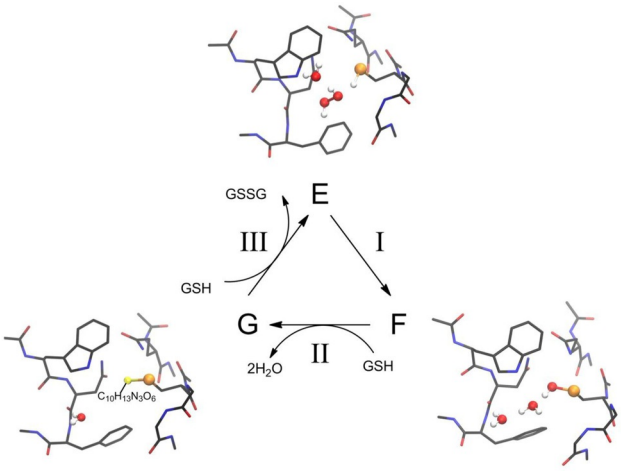

Scheme 1. Mechanism for the reduction of organic hydroperoxides catalyzed by Cys/Sec-GPx. Species **E** is the reduced enzyme with Cys/Sec in the thiol/selenol form, **F** represents the oxidized intermediate, that is, the sulfenic/selenenic acid form, and **G** is the disulfide/selenosulfide form.

in and glutaredoxin as electron donors.[14] GPx4 (or phospholipid hydroperoxide GPx),[11,15] as opposed to the other three GPxs being tetrameric, is a monomer. Its peculiarity is that it can be reduced by a range of different substrates other than GSH. The important role of GPx proteins has encouraged researchers to investigate the role of selenium in this class of enzymes and to design and create molecules that can mimic the activity of these proteins.[16–20]

An analogous mechanism (Scheme 1) can be postulated for the sulfur mutant (Cys-GPx), the antioxidant activity of which is lower than that of Sec-GPx.[21] Recent mechanistic studies, based on DFT calculations on a cluster of seven amino acids forming the catalytic site of GPx, revealed that an identical mechanism could indeed be invoked to explain the enzymatic activities of Cys-GPx and Sec-GPx, and the different energetics (barriers and stabilities of intermediates) along the reaction path showed that the presence of selenium was rate accelerating.[22] Pioneering mechanistic investigations of Sec-GPx were conducted by Morokuma and co-workers,[23] who used pure quantum mechanical methods on a simplified model cluster based on human GPx3 and used a hybrid quantum mechanics/molecular mechanics (QM/MM) scheme on the whole enzyme.[24] Besides selenocysteine, its active site was found to contain Gly50, Leu51, Tyr48, Gln83, and Trp157, modeled as formamide and indole, respectively, plus one to two water molecules. For the oxidation, they proposed a two-step mechanism in addition to a direct mechanism, and the former implied the transfer of the selenol proton to Gln83 and the reduction of the peroxide/formation of **F**. The computed activation energy was in the range of 17.1 to 19.1 kcal mol^{-1}, depending on the mechanism, and was comparable to the value estimated by the authors from the experimental kinetic constant, that is, 14.9 kcal mol^{-1}.[25]

If selenium remains a rare element in biological systems (the maximum number of selenoproteins in vertebrates is 40, whereas thiol-containing proteins are in the thousands, and the limited presence of selenium is ascribed to the high reactivity of selenol in physiological conditions),[3] no trace is found of tellurium in natural proteins. However, tellurocysteine (Tec) has been successfully incorporated in subtilisin to form a semisynthetic protein,[26] and more recently, it was used to replace Ser9 of glutathione transferase from *Lucilia cuprina* to form telluro-LuGST-1.[27] In both cases, remarkable peroxidase activity was reported. This is in agreement with the promising results obtained on the antioxidant efficiency of organotellurides, which have paved the route for their use as drugs.[18,28] In fact, their toxicity seems to be comparable to that of organoselenides,[29] which have been studied for a few decades and represent the paradigmatic GPx mimics. High peroxidase efficiency has also been reported for a cyclodextrin-derived tellurium compound.[30]

In synergy with the syntheses and all the experimental effort, the structure and reactivity of selenium and tellurium enzymes can be theoretically investigated by combining classical and quantum mechanical (QM) methodologies. The computational approach is a powerful tool, provided suitably tailored protocols are used, that is, accurate force-field parameters for molecular dynamics (MD) simulations, which are indispensable to obtain a relaxed equilibrium structure of the whole enzyme, and high levels of theory for the QM calculations, that is, state-of-the-art functionals combined with sufficiently flexible and polarized basis sets. Due to the lack of a force field for Sec and Tec, most classical simulations have been traditionally performed by replacing selenium with sulfur, eventually adjusting the atomic charges,[31–34] or, if parameterization for selenium was undertaken, it was not specific for a single form of Sec but encompassed various oxidation states.[35,36] This approach, although adequate to perform hybrid QM/MM calculations of Sec-containing proteins, as performed by Morokuma and co-workers on GPx systems,[24] is not flexible enough to identify the different behaviors of the chalcogens in the catalytic site. Thus, in this work, we first accurately parametrized the Sec and Tec residues, adjusting the whole set of parameters of their AMBER (assisted model builder with energy refinement) potentials. They were used to simulate the GPx, starting from the crystallographic structure of GPx4, but, due to their flexibility, in the future they may be broadly employed to run MD simulations of different natural and artificial seleno- and telluroproteins. Subsequently, focusing on the catalytic pocket extracted from an MD snapshot, we investigated in detail the initial step of the peroxidase cycle, that is, the oxidation of the Cys, Sec, or Tec center by H_2O_2. The role of the different chalcogens on the energetics and on the reaction mechanism is described, analyzed through activation strain analysis (ASA) for quantitative comparison, and discussed.

2. Results and Discussion

After simulation for 500 ns (Figure 1 a), upon inspection of the positions of the atoms, the structures of the proteins are well maintained and substitution of the chalcogen in residue 46 implies only slight differences. The root-mean-square deviations of the backbone atoms for Sec-GPx and Tec-GPx with respect

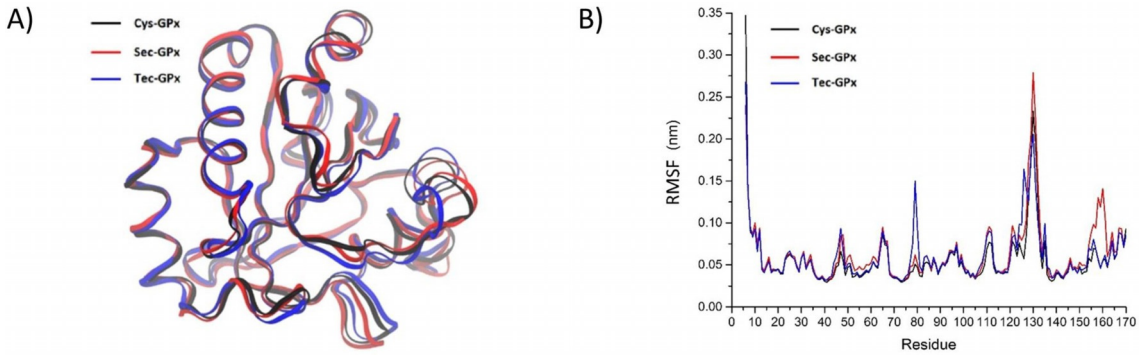

Figure 1. MD results: a) position of the backbone atoms of Cys-GPx, Sec-GPx, and Tec-GPx after 500 ns, and b) root-mean-square fluctuation for each residue along the 500 ns dynamics of Cys-GPx, Sec-GPx, and Tec-GPx.

to Cys-GPx at 500 ns are equal to 0.99 and 1.18 Å, respectively. Moreover, the analysis of the root-mean-square fluctuation (Figure 1 b) shows that the local flexibility for each residue is quite similar, with differences for residue 79 of Tec-GPx, which is a Gly in proximity to the catalytic pocket. This significant change with respect to the Cys and Sec clusters involving a residue that has low conformational freedom arises from the fact that the loop in which the residue is found rotates back and forth by approximately 90° in Tec-GPx during the simulation (Figure S2, Supporting Information). Furthermore, the loop 156–160 of Sec-GPx, which lies far from the catalytic site, also experiences an important rearrangement during the dynamics. Moreover, these simulations corroborate the fact that the active site is accessible to water, as H_2O molecules easily enter and exit from the catalytic pocket. This supports the choice to add one water molecule to investigate the oxidation mechanism, which allows deprotonation of the catalytic Cys/Sec, as the anion is the form prevalent at physiological pH values in natural GPx.[22]

A cluster of seven amino acids was extracted from each simulation (Cys cluster, Sec cluster, and Tec cluster) that was representative of the catalytic pocket.[37] An analogous cluster, fully optimized in the gas phase at the B3LYP/6-31G(d,p) level, was recently used in a pure DFT study of the Cys- and Sec-GPx mechanism.[22] H_2O_2 and H_2O molecules were manually inserted into the Cys, Sec, and Tec clusters, and these initial adducts ($\mathbf{E}\cdot H_2O\cdot H_2O_2$) were optimized (Figure 2). They lie at −2.4, −8.9, and −8.2 kcal mol^{-1} with respect to the free reactants, that is, enzymatic cluster **E** and the H_2O_2 and H_2O molecules (Table 1), which indicates that the catalytic pocket is in all cases suitably tailored to coordinate the substrate and water, which form a hydrogen-bonding network with the surrounding residues (see below). The distance of the chalcogenol proton from the closest oxygen atom of H_2O_2 is significantly different in the three optimized clusters. In the Cys and Sec clusters, distances of 2.29 and 2.15 Å are measured, respectively. In the Tec cluster, a distance of 4.03 Å is found, which precludes any significant in-

Table 1. Gibbs free energies of the intermediates and transition states in the gas phase and in the condensed phase; level of theory: (SMD-)B3LYP-D3(BJ)/6-311 + G(d,p),cc-pVTZ(-PP)// B3LYP-D3(BJ)/6-311G(d,p),cc-pVTZ(-PP).

	Gibbs free energy [kcal mol^{-1}]					
	Gas phase			Condensed phase		
	Cys cluster	Sec cluster	Tec cluster	Cys cluster	Sec cluster	Tec cluster
E	0.0	0.0	0.0	0.0	0.0	0.0
$\mathbf{E}\cdot H_2O\cdot H_2O_2$	−0.4	−4.0	−0.8	−2.4	−8.9	−8.2
TS_1	25.3	16.6		24.7	12.7	
$\mathbf{E}\cdot(CS)\cdot H_2O\cdot H_2O_2$	16.8	5.4		15.9	2.5	
F	−50.2	−73.6		−51.3	−77.3	

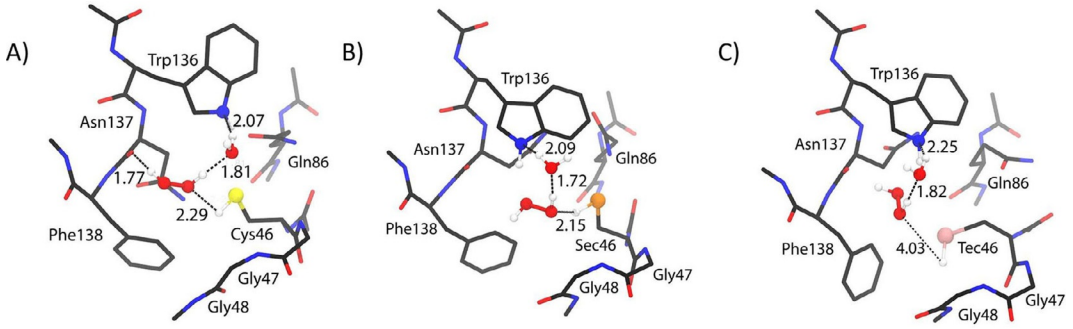

Figure 2. Geometries of the optimized adducts $\mathbf{E}\cdot H_2O_2\cdot H_2O$: a) E = Cys-E RMSD = 0.68 Å, b) E = Sec-E RMSD = 0.85 Å, and c) E = Tec-E RMSD = 0.55 Å.Root-mean-square deviations (RMSDs) (Å, hydrogen atoms not included) are calculated with respect to the initially optimized clusters without including hydrogen atoms. Level of theory: B3LYP-D3(BJ)/6-311G(d,p),cc-pVTZ(-PP).

teraction between the tellurol moiety and H_2O_2 with consequences on the oxidation mechanism (see below).

Focusing on the Cys and Sec clusters, similarities are found in the positions of the H_2O_2 and H_2O molecules (Figure 2a, b). The former is always located between the chalcogen atom and the indole moiety of Trp136. Furthermore, in the case of the Cys cluster, a hydrogen bond between H_2O_2 and the carbonyl oxygen atom of the bond between Asn137 and Phe138 is present. This interaction is absent in the Sec cluster due to the distance of the two groups. In fact, in the optimized structure of the Sec cluster, H_2O_2 is positioned too far from the carbonyl group of the bond between Asn137 and Phe138 for efficient interaction. Conversely, in this case, the increased propinquity to the indole moiety of Trp136 allows interaction of the peroxide oxygen atom with the hydrogen atom bonded to the indole nitrogen atom in Trp136. The H_2O molecule is found to occupy a similar position in both the Cys and Sec clusters, that is, it is located between H_2O_2 and the indole moiety of Trp136; its oxygen atom interacts with a hydrogen atom of the former, and one of its protons points towards the latter. Thus, in both the Cys and Sec clusters a network exists that connects Cys/Sec, H_2O_2, H_2O, and Trp136, and this suggests a viable path for long-range proton transfer. The presence of the water molecule is crucial to deprotonate the chalcogenol. In fact, the thiol/selenol proton is shuttled by proton exchange with the peroxide and water to the indole nitrogen atom of Trp, and a charge-separated intermediate, **E**(CS)·H_2O·H_2O_2, forms. The barrier computed for this process is lower for the Sec cluster than for the Cys cluster, that is, 21.6 vs. 27.1 kcal mol^{-1}, and the product is much less destabilized in the presence of the heavier chalcogen. The conversion into **F** occurs in both cases with negligible activation energy, as no transition state is located, and this is consistent with that previously reported for a similar cluster.[22]

Contrarily, all attempts to verify an analogous mechanism for the Tec cluster failed. This is not surprising: although sulfur and selenium have similar electronegativities, and in both cases the electronegativities are larger than that of hydrogen, tellurium has a much lower electronegativity, and its electronegativity is slightly lower than that of hydrogen; this implies that the Te–H bond is not polarized, and so, the hydrogen atom has no tendency to move to an adjacent oxygen atom. Thus, for the Tec cluster we investigated a different oxidation mechanism that required only the presence of H_2O_2. We found that the direct oxidation to a telluroxide intermediate was possible and that it was the result of nucleophilic attack of the tellurium nucleus to the peroxide. The activation energy (10.5 kcal mol^{-1}, Table 2) is much lower than that required for the formation of the charge-separated intermediates in the Cys and Sec clusters (27.1 and 21.6 kcal mol^{-1}, respectively). This oxidation results in the formation of a strongly stabilized (−43.6 kcal mol^{-1}) telluroxide [**E**-Te(O)H]. An analogous reaction mechanism was proposed for the direct oxidation of numerous selenides and diselenides.[38–41] The telluroxide **E**-Te(O)H can then be converted into tellurenic acid **F**, which is further stabilized by −28.4 kcal mol^{-1} via an isomerization transition state (TS_{iso}) with a barrier of 32.1 kcal mol^{-1}.

Table 2. Gibbs free energies of the intermediates and transition states for the oxidation and isomerization of the Tec cluster in the gas and condensed phases; level of theory: (SMD-B3LYP-D3(BJ)/6-311+G(d,p),cc-pVTZ-PP//B3LYP-D3(BJ)/6-311G(d,p),cc-pVTZ-PP.

	Gibbs free energy [kcal mol^{-1}]	
	Gas phase	Condensed phase
E+H_2O_2	0.0	0.0
E·H_2O_2	−4.3	−4.4
TS_{direct}	6.6	6.1
E-Te(O)H	−41.9	−43.6
TS_{iso}	−10.4	−11.5
F	−72.5	−72.0

Given that tellurium is present in the highly oxidized form of tellurinic acid in two semisynthetic telluroenzymes[26,27] and that the peroxidase cycle can proceed from the telluroxide as well as from the tellurenic or tellurinic species upon reaction with GSH, we also investigated the formation of the tellurinic intermediate **E**-Te(O)OH, which may form in excess amount of the peroxide.

Two possible mechanisms were investigated for the formation of tellurinic acid, the first proceeding in a single step with direct formation of the product (Scheme 2a) and the second

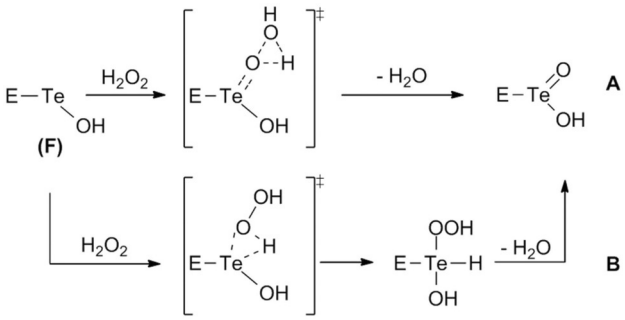

Scheme 2. Mechanism for the formation of tellurinic acid through a) a direct pathway and b) a hydroxy perhydroxy tellurane intermediate.

consisting of a two-step path that involves the intermediate formation of a hydroxy perhydroxy tellurane (Scheme 2b). On the basis of the energetics, the stepwise mechanism is disfavored over the direct oxidation (Table 3), in analogy with results recently reported for the oxidation of organic selenides

Table 3. Gibbs free energies for the two possible mechanisms for tellurinic acid formation shown in Scheme 2; level of theory: SMD-B3LYP-D3(BJ)/6-311+G(d,p),cc-pVTZ-PP//B3LYP-D3(BJ)/6-311G(d,p),cc-pVTZ-PP.

	Gibbs free energy [kcal mol^{-1}]	
	Path A	Path B
F+H_2O_2	0.0	0.0
F·H_2O_2	−3.8	−3.8
TS	12.9	29.3
E-Te(OH)(OOH)H	–	2.9
E-Te(O)OH	−52.6	−52.6

by H_2O_2.[41] In fact, an activation energy of 16.7 kcal mol^{-1} is computed for the direct oxidation versus a barrier of 33.1 kcal mol^{-1} for the formation of the hydroxy perhydroxy tellurane. In addition, the latter is less stable than the starting structure by 6.7 kcal mol^{-1}. As predicted, the most stable species, lying at −52.6 kcal mol^{-1}, is the tellurinic acid (Figure 3). On the basis of the energetics, we believe that either the telluroxide or the tellurinic acid is a good candidate for subsequent nucleophilic attack of GSH.

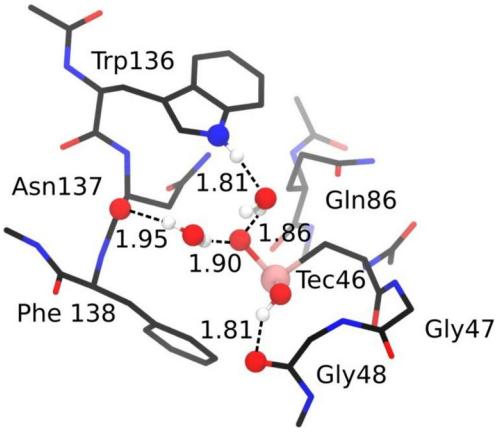

Figure 3. Optimized Tec cluster in the tellurinic acid form [**E**-Te(O)OH] and relevant interatomic distances [Å]. Level of theory: B3LYP-D3(BJ)/6-311G(d,p),cc-pVTZ-PP.

To elucidate the origin of the difference in activation energies for the oxidation of the Cys and Sec clusters, ASA and energy decomposition analysis (EDA) in the gas phase were employed (see DFT calculations in the Methods Section). Single-point calculations were performed on the previously optimized B3LYP-D3(BJ)/6-311G(d,p),cc-pVTZ geometries. The Cys and Sec clusters were divided into two fragments (Scheme 3, case I): the first one comprised Cys/Sec46, Gly47, and Gly48

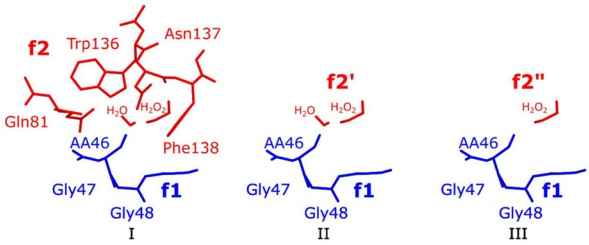

Scheme 3. Different partitioning of the Cys and Sec clusters; AA46 = Cys46, Sec46.

(**f1**), and the second contained the remaining residues, namely, Gln81, Trp136, Asn137, Phe138, the water molecule, and the hydrogen peroxide molecule (**f2**). As the difference in efficiencies between selenium and sulfur in the oxidation is related to the smaller barrier for the formation of TS_1, we focused the ASA on the initial adduct and TS_1. A preliminary benchmark ASA was conducted to compare the results among different levels of theory, namely, B3LYP-D3(BJ)/6-311+G(d,p),cc-pVTZ//B3LYP-D3(BJ)/6-311G(d,p),cc-pVTZ; ZORA-BLYP-D3(BJ)/TZ2P//B3LYP-D3(BJ)/6-311G(d,p),cc-pVTZ; and ZORA-B3LYP/TZ2P//B3LYP-D3(BJ)/6-311+G(d,p),cc-pVTZ. Given that the results are comparable for all of these different functionals (see the Supporting Information), we chose to perform these analyses with ZORA-BLYP-D3(BJ)/TZ2P, as implemented in the Amsterdam density functional (ADF) program. This level of theory proved to be reliable to calculate the energies of the organochalcogen compounds.[42]

Focusing the discussion first on case I, which corresponds to the whole Sec/Cys cluster partitioned as shown in Scheme 3, **E**·H_2O_2·H_2O is less stabilized with respect to the free reactants in the Cys cluster (−12.9 kcal mol^{-1}) than in the Sec cluster (−19.2 kcal mol^{-1}). This is essentially due to a much larger strain contribution, that is, 11.8 vs. 3.0 kcal mol^{-1} (Table 4). However, the stabilization of these initial adducts indicates a favorable interplay between the substrate and the residues in

Table 4. ASA and EDA (in kcal mol^{-1}) for the Cys and Sec clusters.[a]

					Cys					
		ΔE	ΔE_{strain}(**f1**)	ΔE_{strain}(**f2**)	ΔE_{strain}	ΔE_{int}	ΔE_{Pauli}	ΔV_{elst}	ΔE_{oi}	ΔE_{disp}
f2	Adduct	−12.9	5.0	6.8	11.8	−24.7	36.9	−22.9	−12.8	−25.9
	TS_1	8.4	59.4	36.6	96.0	−87.6	246.8	−119.6	−188.8	−26.0
f2′	Adduct	1.9	5.0	0.6	5.6	−3.7	6.8	−5.2	−2.4	−2.9
	TS_1	44.8	59.4	33.8	93.2	−48.4	207.1	−95.7	−157.0	−2.8
f2″	Adduct	3.1	5.0	−0.2	4.8	−1.7	5.7	−3.4	−2.1	−1.9
	TS_1	68.6	59.4	27.6	87.0	−18.4	206.0	−84.1	−138.3	−2.0
					Sec					
		ΔE	ΔE_{strain}(**f1**)	ΔE_{strain}(**f2**)	ΔE_{strain}	ΔE_{int}	ΔE_{Pauli}	ΔV_{elst}	ΔE_{oi}	ΔE_{disp}
f2	Adduct	−19.2	1.2	1.8	3.0	−22.2	35.1	−23.1	−13.7	−20.5
	TS_1	−2.5	27.9	31.6	59.5	−62.0	207.6	−105.2	−143.8	−20.6
f2′	Adduct	−4.0	1.2	1.0	2.2	−6.2	9.4	−8.4	−4.2	−3.0
	TS_1	29.3	27.9	36.2	64.1	−34.8	176.5	−85.9	−121.8	−3.6
f2″	Adduct	−2.5	1.2	0.0	1.2	−3.7	10.4	−6.7	−3.2	−4.2
	TS_1	50.9	27.9	31.5	59.4	−8.5	173.1	−73.1	−105.2	−3.3

[a] Electronic energies in the gas phase, computed at ZORA-BLYP-D3(BJ)/TZ2P//B3LYP-D3(BJ)/6-311G(d,p),cc-pVTZ.

the catalytic pocket in both clusters. The height of the barrier for the elementary step leading to the charge-separated intermediate **E**(CS)·H_2O·H_2O_2 depends on the location of the transition state on the potential-energy surface. The strain contribution to the energy of TS_1 is much larger for the Cys cluster than for the Sec cluster (96.0 vs. 59.5 kcal mol^{-1}), and the corresponding interaction contributions (−87.6 and −62.0 kcal mol^{-1}) compensate for it only in the latter case, mainly due to a much more stabilizing orbital interaction (ΔE_{oi}) (−143.8 vs. −188.8 kcal mol^{-1}). This results in an activation energy for the process of thiol/selenol proton transfer to Trp136 that is larger for the Cys cluster than for the Sec cluster (21.3 vs. 16.7 kcal mol^{-1}, in the gas phase), which is analogous to what we computed from the data in solution (Table 1). The large strain in the transition state of the Cys cluster is due to stronger variation in the S–H bond length, which amounts to 0.66 Å, compared to variation in the Se–H distance in TS_1 of the Sec cluster, which is 0.47 Å, and thus, the strain is related to the nature of the chalcogen nucleus.

To investigate the role of amino-acid residues other than Cys/Sec, the analysis was repeated after simplifying the second fragment **f2**: by removing all the protein residues, a fragment containing H_2O and H_2O_2 was left (**f2′**); by also removing the water molecule, only the oxidant H_2O_2 (**f2″**) remained. These fragments are shown in Scheme 3, cases II and III.

In both cases, for the Cys cluster, the initial adduct is not energetically stabilized with respect to the free reactants, that is, 1.9 and 3.1 kcal mol^{-1} (Table 4), and for the Sec cluster, the stabilization decreases significantly relative to that of the full system and arrives at −4.0 and −2.5 kcal mol^{-1}. This result denotes the important effect of the removed protein residues, that is, Gln81, Trp136, Asn137, and Phe138 upon going from **f2** to **f2′** and **f2″**. In fact, the first three amino-acid residues, together with Cys/Sec46, have been experimentally identified as the "catalytic tetrad", whereas Phe138 is a conserved residue.[37] The slight stabilization computed for the Sec cluster in cases II and III is due to larger interaction and smaller strain relative to the analogous cases for the Cys cluster. The barriers for proton transfer largely increase upon removal of the protein residues, that is, upon going from case I to case II due to strong destabilization of the transition states for the Cys cluster as well as for the Sec cluster in case I. The strain energy (ΔE_{strain}) values of the transition states do not change much (96.0 to 93.2 kcal mol^{-1} and 59.5 to 64.1 kcal mol^{-1}, respectively). In contrast, the interaction energy (ΔE_{int}) weakens significantly (from −87.6 to −48.4 kcal mol^{-1} and from −62.0 and −34.8 kcal mol^{-1}, respectively), mainly due to weakening of electrostatic attraction (ΔV_{elst}) and ΔE_{oi}. The activation energy is again higher for the Cys cluster than for the Sec cluster, that is, 42.9 and 33.3 kcal mol^{-1}. Upon also removing the water molecule, that is, reducing **f2′** to **f2″** (Scheme 3, case III), the same observations subsist for the strain and interaction contributions to the energy of TS_1 and to the trend of the barrier height: the latter increases to 65.5 kcal mol^{-1} in the Cys cluster and to 53.4 kcal mol^{-1} in the Sec cluster. Importantly, we conclude that the presence of the water molecule has a role in lowering the activation energy of the proton-transfer process.

3. Conclusions

The mechanism of oxidation of the catalytic site of human peroxidase by H_2O_2 was investigated in silico with state-of-the-art combined classical mechanics and quantum chemistry methodologies. In particular, the mechanistic details of the cysteine (Cys), selenocysteine (Sec), and tellurocysteine (Tec) active sites were systematically investigated to assess the role of the different chalcogens in the oxidation step.

For Cys and Sec, an analogous mechanism was validated, and the formation of a charge-separated intermediate with a thiolate/selenolate center and with more favorable energetics for the Sec-glutathione peroxidase (GPx) was predicted. In contrast, for Tec-GPx, all attempts to find a similar path on the potential-energy surface failed. In this last case, direct oxidation was found to be energetically favored, which led to the formation of a telluroxide intermediate that could either be directly attacked by glutathione (GSH) or isomerized to tellurenic acid (TeOH). Alternatively, oxidation with a second equivalent of H_2O_2 converted the telluroxide into the tellurinic form, which was the resting state of both the artificial telluroenzymes characterized so far. The mechanistic differences and the favorable energetics encountered for Tec-GPx explain the strong peroxidase activity reported for artificial Tec enzymes and prompts for more effort in this research field.

Activation strain analyses performed for the Cys and Sec clusters showed that the more favorable initial oxidation of the Sec cluster was mainly due to the balance between strain and interaction energy, which gave rise to a smaller activation barrier than that found for the Cys cluster. The main reason for this was the smaller relative and absolute elongation of the Se–H bond in the Sec cluster (compared to the S–H bond in the Cys cluster), which translated into less activation strain and thus a lower barrier for the reaction involving Sec.

Methods

MD Simulations

The GPx4 structure was chosen as a model structure for a peroxidase enzyme (PDB entry: 2OBI).[43] To run MD simulations, we chose the assisted model builder with energy refinement (AMBER) Hamiltonian ff14SB,[44] implemented in the Amber 2015 software package,[45] due to its good performance in treating biomolecules [Eq. (1)].

$$V_{AMBER} = \sum_{i<j}^{n'_{atoms}} \frac{q_i q_j}{4\pi\varepsilon_0 r_{ij}} + \sum_{i<j}^{n'_{atoms}} 4\epsilon_{ij}\left[\left(\frac{\sigma_{ij}}{r_{ij}}\right)^6 - \left(\frac{\sigma_{ij}}{r_{ij}}\right)^{12}\right] + \sum_{i}^{n_{bonds}} b_i\left(r_i - r_{i,eq}\right)^2 + \sum_{i}^{n_{angles}} a_i\left(\theta_i - \theta_{i,eq}\right)^2 + \sum_{i}^{n_{dihedrals}} \sum_{n}^{n_{i,max}} \frac{V_{i,n}}{2}\left[1 + \cos\left(n\phi_i - \gamma_{i,n}\right)\right] \quad (1)$$

In Equation (1), the first two terms represent the electrostatic and Lennard–Jones potential for nonbonded forces, respectively (the index n'_{atoms} indicates only those atom pairs that belong to different molecules or are separated by a minimum of three bonds),

and the last three terms indicate harmonic potential contributions for bonds (r) and angles (θ) and a truncated Fourier series for dihedrals (ϕ). Simulations were straightforward for Cys-GPx, because all the necessary parameters were already available in ff14SB.[44] On the other hand, for the Sec- and Tec-based enzymes, no suitable parameters were available. Thus, we chose to derive the missing parameters for these residues by using a protocol and tools recently employed by some of us to derive GAFF (General AMBER Force Field) parameters for a series of organochalcogen compounds.[46]

Charges were calculated by using R.E.D Server Development,[47] which is a web-based interface that employs the PyRED program[48] and R.E.D tools.[49] Calculations were performed, as recommended,[50] at the Hartree–Fock level of theory by using the 6-31G(d) basis set for all the atoms except tellurium, for which the Stuttgart Dresden effective core potential basis set[51,52] was employed; the Gaussian 09 package was used for these calculations.[53] To cover the energetically relevant conformations of Sec and Tec, the nine most stable conformers were selected, according to a previous systematic conformational study of cysteine.[54] For Sec and Tec, the nine conformers, generated by replacing sulfur with selenium and tellurium, respectively, were fully optimized by using B3LYP,[55–58] as implemented in Gaussian 09, combined with cc-pVTZ basis sets for all the atoms (level of theory: B3LYP/cc-pVTZ); for tellurium a pseudopotential was used (level of theory: B3LYP/cc-pVTZ,cc-pVTZ-PP). To obtain highly reproducible charges, two different orientations were taken into account for each conformer by using the rigid-body reorientation algorithm implemented in R.E.D. Tools.[49] The final charge values for each amino acid resulted from a simultaneous restrained electrostatic potential (RESP)[50] fit of 18 structures.

For Lennard–Jones σ and ε parameters, we used 2.1200 Å and 0.2910 kcal mol^{-1} for Se and 2.2600 Å and 0.3980 kcal mol^{-1} for tellurium, consistent with previous work.[46] During the simulation, they were combined according to the Lorentz–Berthelot mixing rules.

Constrained scans (i.e. calculations for which only the relevant parameter was changed and the rest of the molecule was kept frozen) were performed at B3LYP/cc-pVTZ (cc-pVTZ-PP for Tec) to obtain the force constants of the harmonic contributions [i.e. a_i and b_i terms in Eq. (1)]. Stretching and bending parameters were thus computed for CB–X and X–HG bonds (X = Se, Te) and for CA–CB–X, CB–X–HG, and HB2–CB–X angles, respectively (Scheme 4). Relaxed scans for each of the nine conformers used in atomic charges derivation were performed for the dihedrals CA–CB–X–HG and HB2–CB–X–HG, the parameters of which were absent in ff14SB (Scheme 4). Moreover, although generalized parameters for dihedrals N–CA–CB–X and C–CA–CB–X, in which the chalcogen atom is in the terminal position, were already present in ff14SB, we

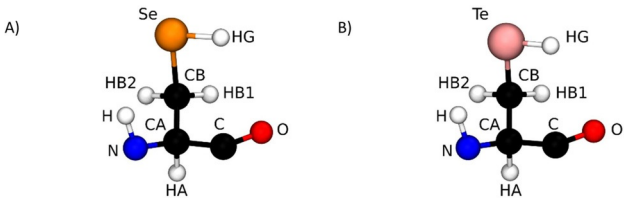

Scheme 4. Atom numbering scheme of the parametrized residues: a) Sec and b) Tec.

decided to improve these data by refitting the coefficients. The energies of the resulting ensemble of 720 structures were simultaneously fit with Paramfit,[59] a tool included in Ambertools15. The results of this fitting are shown in Figure S1. The new parameters were employed in the MD simulations of the Sec-GPx and Tec-GPx. The initial structures of Cys-GPx, Sec-GPx, and Tec-GPx were solvated with TIP3P water (6942 water molecules for Cys-GPx, 6946 for Sec-GPx, and 7121 for Tec-GPx).[60] Afterwards, the systems were minimized and equilibrated for 200 ps at 300 K and 0.101 MPa. The MD simulations were performed for 500 ns under the same conditions of the equilibration by using a Langevin thermostat and a Monte Carlo barostat.

DFT Calculations

A suitable enzymatic cluster was chosen to represent the GPx active site. Seven residues (Cys/Sec/Tec46, Gly47, Lys48, Gln81, Trp136, Asn137, and Phe138) were selected, in agreement with previous work.[22] The initial structures were retrieved from a snapshot of the MD simulations and were optimized by keeping the backbone atoms frozen to avoid loss of the structural effects of the large portion of GPx excluded from QM computations (Figure 4a). The extracted residues were suitably capped by using ACE [$C(O)CH_3$] and NME [$N(H)CH_3$] groups at the N- and C-terminal positions, respectively, to simulate the removed protein chain. Lys48 was substituted with a Gly residue to reproduce a peptide bond connecting Gly47 to the nonconserved following residues (Figure 4b).[22] The dispersion-corrected hybrid B3LYP-D3(BJ)[55–58] functional was used, as implemented in the Gaussian 09 software. It comprises the Becke three parameter functional[55] and the Lee, Yang, and Parr[56,61,62] correlation term with an added dispersion contribution term developed by Grimme et al.[63]

The 6-311G(d,p) basis set was used for all atoms, except selenium and tellurium, for which Dunning's correlation consistent basis set of triple ζ quality (cc-pVTZ) was used; for tellurium, pseudopotentials were also included (cc-pVTZ-PP). The level of theory employed

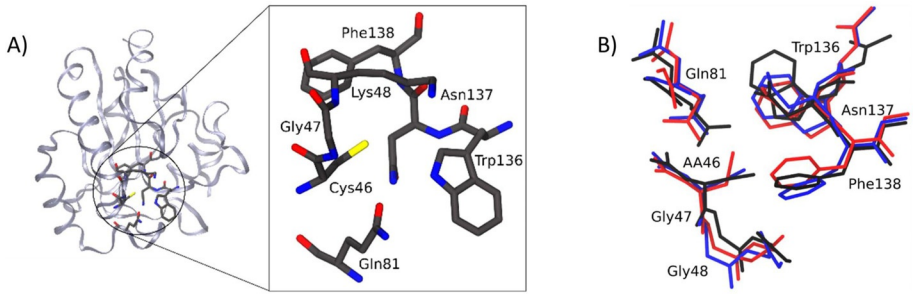

Figure 4. a) Cluster of amino acids extracted from Cys-GPx and b) superposition of the optimized geometries of the Cys (black), Sec (red), and Tec GPx (blue) clusters; AA46 = Cys46, Sec46, and Tec46. Level of theory: B3LYP-D3(BJ)/6-311G(d,p),cc-pVTZ(-PP).

for partially constrained geometry optimizations is denoted B3LYP-D3(BJ)/6-311G(d,p),cc-pVTZ(-PP). Frequencies calculations were subsequently performed to verify the absence of imaginary frequencies for minima and the presence of a single imaginary frequency for transitions states, associated to the correct vibrational mode. Single-point energy calculations were performed in the gas phase at B3LYP-D3(BJ)/6-311+G(d,p),cc-pVTZ(-PP), and the correction for the condensed phase was computed by using the SMD solvation model [SMD- B3LYP-D3(BJ)/6-311G(d,p),cc-pVTZ(-PP)] as implemented in Gaussian 09.[64,65] A dielectric constant of 4.0 was employed to reproduce the protein environment, in agreement with previous studies.[66] Thermodynamic corrections resulting from gas-phase frequency calculations (same level of theory employed in the geometry optimizations) were added; they refer to a temperature of 298.15 K and a pressure of about 0.1 MPa.[67] If not differently stated, Gibbs free energies in condensed phase are discussed in the Results section.

The activation strain analysis (ASA)[68,69] was employed to analyze more quantitatively the reaction potential-energy surface (PES) of the oxidation of Cys-**E** and Sec-**E**. In this model, the system is partitioned into two fragments and the total energy (ΔE) is decomposed into the sum of strain energy (ΔE_{strain}) and interaction energy (ΔE_{int}) [Eq. (2)]:

$$\Delta E = \Delta E_{strain} + \Delta E_{int} \quad (2)$$

where ΔE_{strain} is the energy associated with deforming the fragments from their isolated geometry into the geometry they acquire in the system at equilibrium. It can be divided into a contribution stemming from each reactant. ΔE_{int} is the actual interaction energy between the deformed reactants, which can also be further analyzed in the framework of the Kohn–Sham molecular orbital (MO) model by using quantitative energy decomposition analysis (EDA) of the bond into electrostatic attraction (ΔV_{elst}), Pauli repulsion (or exchange repulsion ΔE_{Pauli}), and stabilizing orbital interactions (ΔE_{oi}), further augmented with Grimme's D3 dispersion energy (ΔE_{disp}) [Eq. (3)]:

$$\Delta E_{int} = \Delta V_{elst} + \Delta E_{Pauli} + \Delta E_{oi} + \Delta E_{disp} \quad (3)$$

For these analyses, the Amsterdam density functional (ADF) program was used.[70–73] In these calculations, scalar relativistic effects were accounted for through the zeroth-order regular approximation (ZORA).[74] The BLYP[56,61,62,75] functional was used, in combination with the TZ2P basis set for all elements. The TZ2P basis set is a large uncontracted set of Slater-type orbitals (STOs), of triple-ζ quality and augmented with two sets of polarization functions on each atom: 2p and 3d in the case of hydrogen; 3d and 4f in the cases of carbon, nitrogen, oxygen, and sulfur; and 4d and 4f in the case of selenium. Dispersion corrections were included with the D3 scheme with inclusion of the Becke Johnson damping [D3(BJ)], developed by Grimme et al.[63] This level of theory is denoted ZORA-BLYP-D3(BJ)/TZ2P.

Acknowledgements

Calculations were performed on Galileo (CINECA: Casalecchio di Reno, Italy) thanks to the ISCRA Grant DAISIES (Developing Antioxidant Innovative Solutions Inspired by Enzymatic Systems) and on the C3P clusters (Dipartimento di Scienze Chimiche, Università degli Studi di Padova). L.O. is grateful to Prof. Fulvio Ursini (Dip. Medicina Molecolare, Università degli Studi di Padova) for fruitful discussions on the biological aspects of GPx activity. F.M.B. thanks the Netherlands Organisation for Scientific Research (NWO) for support through the PEPSci program.

Conflict of interest

The authors declare no conflict of interest.

Keywords: activation strain analysis · density functional calculations · enzymes · selenium · tellurium

[1] J. R. Arthur, *Cell. Mol. Life Sci.* **2001**, *57*, 1825–1835.
[2] H. J. Reich, R. J. Hondal, *ACS Chem. Biol.* **2016**, *11*, 821–841.
[3] J. B. T. Rocha, B. C. Piccoli, C. S. Oliveira, *ARKIVOC* **2017**, 457–491.
[4] R. E. Huber, R. S. Criddle, *Arch. Biochem. Biophys.* **1967**, *122*, 164–173.
[5] R. J. Hondal, E. L. Ruggles, *Amino Acids* **2011**, *41*, 73–89.
[6] E. S. J. Arnér, *Exp. Cell Res.* **2010**, *316*, 1296–1303.
[7] S. M. Kanzok, *Science* **2001**, *291*, 643–646.
[8] F. M. Maiorino, R. Brigelius-Flohé, K. D. Aumann, A. Roveri, D. Schomburg, L. Flohé, *Methods Enzymol.* **1995**, *252*, 38–48.
[9] L. Flohé, *Methods Enzymol.* **2010**, *473*, 1–39.
[10] O. Epp, R. Ladenstein, A. Wendel, *Eur. J. Biochem.* **1983**, *133*, 51–69.
[11] F. Ursini, M. Maiorino, C. Gregolin, *Biochim. Biophys. Acta Gen. Subj.* **1985**, *839*, 62–70.
[12] G. C. Mills, *J. Biol. Chem.* **1957**, *229*, 189–197.
[13] F. F. Chu, J. H. Doroshow, R. S. Esworthy, *J. Biol. Chem.* **1993**, *268*, 2571–2576.
[14] M. Bjornstedt, J. Y. Xue, W. H. Huang, B. Akesson, A. Holmgren, *J. Biol. Chem.* **1994**, *269*, 29382–29384.
[15] M. Maiorino, V. Bosello-Travain, G. Cozza, G. Miotto, L. Orian, A. Roveri, S. Toppo, M. Zaccarin, F. Ursini in *Selenium: Its Molecular Biology and Role in Human Health* (Eds.: D. L. Hatfield, U. Schweizer, P. A. Tsuji, V. N. Gladyshev), Springer, Berlin, **2016**, pp. 223–234.
[16] K. P. Bhabak, G. Mugesh, *Acc. Chem. Res.* **2010**, *43*, 1408–1419.
[17] Z. Y. Done, X. Huang, S. Z. Mao, K. Liang, J. Q. Liu, G. M. Luo, J. C. Shen, *Chem. Eur. J.* **2006**, *12*, 3575–3579.
[18] C. W. Nogueira, G. Zeni, J. B. T. Rocha, *Chem. Rev.* **2004**, *104*, 6255–6285.
[19] L. Orian, S. Toppo, *Free Radical Biol. Med.* **2014**, *66*, 65–74.
[20] L. P. Wolters, L. Orian, *Curr. Org. Chem.* **2016**, *20*, 189–197.
[21] S. Toppo, L. Flohé, F. Ursini, S. Vanin, M. Maiorino, *Biochim. Biophys. Acta Gen. Subj.* **2009**, *1790*, 1486–1500.
[22] L. Orian, P. Mauri, A. Roveri, S. Toppo, L. Benazzi, V. Bosello-Travain, A. De Palma, M. Maiorino, G. Miotto, M. Zaccarin, A. Polimenoa, L. Flohéc, F. Ursinic, *Free Radical Biol. Med.* **2015**, *87*, 1–14.
[23] R. Prabhakar, T. Vreven, K. Morokuma, D. G. Musaev, *Biochemistry* **2005**, *44*, 11864–11871.
[24] R. Prabhakar, T. Vreven, M. J. Frisch, K. Morokuma, D. G. Musaev, *J. Phys. Chem. B* **2006**, *110*, 13608–13613.
[25] G. Roy, M. Nethaji, G. Mugesh, *J. Am. Chem. Soc.* **2004**, *126*, 2712–2713.
[26] S. Mao, Z. Dong, J. Liu, X. Li, X. Liu, G. Luo, J. Shen, *J. Am. Chem. Soc.* **2005**, *127*, 11588–11589.
[27] X. Liu, L. A. Silks, C. Liu, M. Ollivault-Shiflett, X. Huang, J. Li, G. Luo, Y. M. Hou, J. Liu, J. Shen, *Angew. Chem. Int. Ed.* **2009**, *48*, 2020–2023; *Angew. Chem.* **2009**, *121*, 2054–2057.
[28] E. R. T. Tiekink, *Dalton Trans.* **2012**, *41*, 6390.
[29] M. Ibrahim, W. Hassan, D. F. Meinerz, M. Dos Santos, C. V. Klimaczewski, A. M. Deobald, M. S. Costa, C. W. Nogueira, N. B. V. Barbosa, J. B. T. Rocha, *Mol. Cell. Biochem.* **2012**, *371*, 97–104.
[30] X. Ren, Y. Xue, J. Liu, K. Zhang, J. Zheng, G. Luo, C. Guo, Y. Mu, J. Shen, *ChemBioChem* **2002**, *3*, 356–363.
[31] H. Zhong, E. W. Taylor, *J. Mol. Graphics Modell.* **2004**, *23*, 223–231.
[32] D. Dimastrogiovanni, M. Anselmi, A. E. Miele, G. Boumis, L. Petersson, F. Angelucci, A. Di Nola, M. Brunori, A. Bellelli, *Proteins Struct. Funct. Bioinf.* **2010**, *78*, 259–270.

[33] O. Gutiérrez-Sanz, M. C. Marques, C. S. A. Baltazar, V. M. Fernández, C. M. Soares, I. A. C. Pereira, A. L. De Lacey, *J. Biol. Inorg. Chem.* **2013**, *18*, 419 – 427.
[34] V. H. Teixeira, A. S. C. Capacho, M. Machuqueiro, *Proteins Struct. Funct. Bioinf.* **2016**, *84*, 1836 – 1843.
[35] S. T. Ali, S. Jahangir, S. Karamat, W. M. F. Fabian, K. Nawara, J. Kóňa, *J. Chem. Theory Comput.* **2010**, *6*, 1670 – 1681.
[36] J. Kóňa, W. M. F. Fabian, *J. Chem. Theory Comput.* **2011**, *7*, 2610 – 2616.
[37] S. C. E. Tosatto, V. Bosello, F. Fogolari, P. Mauri, A. Roveri, S. Toppo, L. Flohé, F. Ursini, M. Maiorino, *Antioxid. Redox Signaling* **2008**, *10*, 1515 – 1526.
[38] E. A. Cowan, C. D. Oldham, S. W. May, *Arch. Biochem. Biophys.* **2011**, *506*, 201 – 207.
[39] K. Arai, K. Dedachi, M. Iwaoka, *Chem. Eur. J.* **2011**, *17*, 481 – 485.
[40] A. S. Hodage, P. P. Phadnis, A. Wadawale, K. I. Priyadarsini, V. K. Jain, *Org. Biomol. Chem.* **2011**, *9*, 2992 – 2998.
[41] G. Ribaudo, M. Bellanda, I. Menegazzo, L. P. Wolters, M. Bortoli, G. Ferrer-Sueta, G. Zagotto, L. Orian, *Chem. Eur. J.* **2017**, *23*, 2405 – 2422.
[42] F. Zaccaria, L. P. Wolters, C. Fonseca Guerra, L. Orian, *J. Comput. Chem.* **2016**, *37*, 1672 – 1680.
[43] P. Scheerer, A. Borchert, N. Krauss, H. Wessner, C. Gerth, W. Höhne, H. Kuhn, *Biochemistry* **2007**, *46*, 9041 – 9049.
[44] J. A. Maier, C. Martinez, K. Kasavajhala, L. Wickstrom, K. E. Hauser, C. Simmerling, *J. Chem. Theory Comput.* **2015**, *11*, 3696 – 3713.
[45] D. A. Case, J. T. Berryman, R. M. Betz, D. S. Cerutti, T. E. Cheatham III, T. A. Darden, R. E. Duke, T. J. Giese, H. Gohlke, A. W. Goetz, N. Homeyer, S. Izadi, P. Janowski, J. Kaus, A. Kovalenko, T. S. Lee, S. LeGrand, P. Li, T. Luchko, R. Luo, B. Madej, K. M. Merz, G. Monard, P. Needham, H. Nguyen, H. T. Nguyen, I. Omelyan, A. Onufriev, D. R. Roe, A. Roitberg, R. Salomon-Ferrer, C. L. Simmerling, W. Smith, J. Swails, R. C. Walker, J. Wang, R. M. Wolf, X. Wu, D. M. York and P. A. Kollman, *AMBER 2015*, University Of California, San Francisco, San Francisco, **2015**.
[46] M. Torsello, A. C. Pimenta, L. P. Wolters, I. S. Moreira, L. Orian, A. Polimeno, *J. Phys. Chem. A* **2016**, *120*, 4389 – 4400.
[47] E. Vanquelef, S. Simon, G. Marquant, E. Garcia, G. Klimerak, J. C. Delepine, P. Cieplak, F. Y. Dupradeau, *Nucleic Acids Res.* **2011**, *39*, W511 – W517.
[48] F. Wang, J. P. Becker, P. Cieplak, F.-Y. Dupradeau, *R. E. D. Python: Object Oriented Programming for AMBER Force Fields*, Université De Picardie—Jules Verne, Sanford Burnham Prebys Medical Discovery Institute, **2013**.
[49] F. Y. Dupradeau, A. Pigache, T. Zaffran, C. Savineau, R. Lelong, N. Grivel, D. Lelong, W. Rosanski, P. Cieplak, *Phys. Chem. Chem. Phys.* **2010**, *12*, 7821 – 7839.
[50] Charges derived at HF/6-31G(d) lead to overestimation of the dipole moment, which thus balances the dipole moment of TIP3P water. C. C. I. Bayly, P. Cieplak, W. D. Cornell, P. A. Kollmann, *J. Phys. Chem.* **1993**, *97*, 10269 – 10280.
[51] G. Igel-Mann, H. Stoll, H. Preuss, *Mol. Phys.* **2006**, *65*, 1321 – 1328.
[52] A. Bergner, M. Dolg, W. Küchle, H. Stoll, H. Preuß, *Mol. Phys.* **1993**, *80*, 1431 – 1441.
[53] Gaussian 09, Revision D.01, M. J. Frisch, G. W. Trucks, H. B. Schlegel, G. E. Scuseria, M. A. Robb, J. R. Cheeseman, G. Scalmani, V. Barone, B. Mennucci, G. A. Petersson, H. Nakatsuji, M. Caricato, X. Li, H. P. Hratchian, A. F. Izmaylov, J. Bloino, G. Zheng, J. L. Sonnenberg, M. Hada, M. Ehara, K. Toyota, R. Fukuda, J. Hasegawa, M. Ishida, T. Nakajima, Y. Honda, O. Kitao, H. Nakai, T. Vreven, J. A. Montgomery, Jr., J. E. Peralta, F. Ogliaro, M. Bearpark, J. J. Heyd, E. Brothers, K. N. Kudin, V. N. Staroverov, R. Kobayashi, J. Normand, K. Raghavachari, A. Rendell, J. C. Burant, S. S. Iyengar, J. Tomasi, M. Cossi, N. Rega, J. M. Millam, M. Klene, J. E. Knox, J. B. Cross, V. Bakken, C. Adamo, J. Jaramillo, R. Gomperts, R. E. Stratmann, O. Yazyev, A. J. Austin, R. Cammi, C. Pomelli, J. W. Ochterski, R. L. Martin, K. Morokuma, V. G. Zakrzewski, G. A. Voth, P. Salvador, J. J. Dannenberg, S. Dapprich, A. D. Daniels, Ö. Farkas, J. B. Foresman, J. V. Ortiz, J. Cioslowski, D. J. Fox, Gaussian, Inc., Wallingford, CT, **2009**.
[54] J. J. Wilke, M. C. Lind, H. F. Schaefer, A. G. Császár, W. D. Allen, *J. Chem. Theory Comput.* **2009**, *5*, 1511 – 1523.
[55] A. D. Becke, *J. Chem. Phys.* **1993**, *98*, 5648.
[56] C. Lee, W. Yang, R. G. Parr, *Phys. Rev. B* **1988**, *37*, 785 – 789.
[57] S. H. Vosko, L. Wilk, M. Nusair, *Can. J. Phys.* **1980**, *58*, 1200 – 1211.
[58] P. J. Stephens, F. J. Devlin, C. F. Chabalowski, M. J. Frisch, *J. Phys. Chem.* **1994**, *98*, 11623 – 11627.
[59] R. M. Betz, R. C. Walker, *J. Comput. Chem.* **2015**, *36*, 79 – 87.
[60] W. L. Jorgensen, J. Chandrasekhar, J. D. Madura, R. W. Impey, M. L. Klein, *J. Chem. Phys.* **1983**, *79*, 926.
[61] B. G. Johnson, P. M. W. Gill, J. A. Pople, *J. Chem. Phys.* **1993**, *98*, 5612 – 5626.
[62] T. V. Russo, R. L. Martin, P. J. Hay, *J. Med. Phys.* **1994**, *101*, 7729 – 7737.
[63] S. Grimme, S. Ehrlich, L. Goerigk, *J. Comput. Chem.* **2011**, *32*, 1456 – 1465.
[64] A. V. Marenich, C. J. Cramer, D. G. Truhlar, *J. Phys. Chem. B* **2009**, *113*, 6378 – 6396.
[65] J. Antony, R. Sure, S. Grimme, *Chem. Commun.* **2015**, *51*, 1764 – 1774.
[66] L. Li, C. Li, Z. Zhang, E. Alexov, *J. Chem. Theory Comput.* **2013**, *9*, 2126 – 2136.
[67] R. F. Ribeiro, A. V. Marenich, C. J. Cramer, D. G. Truhlar, *J. Phys. Chem. B* **2011**, *115*, 14556 – 14562.
[68] F. M. Bickelhaupt, E. J. Baerends in *Reviews in Computational Chemistry* (Eds.: K. B. Lipkowitz, D. B. Boyd), Wiley-VCH, New York, **2001**, Vol. 15, pp. 1 – 86.
[69] I. Fernández, F. M. Bickelhaupt, *Chem. Soc. Rev.* **2014**, *43*, 4953.
[70] E. J. Baerends, D. E. Ellis, P. Ros, *Chem. Phys.* **1973**, *2*, 41 – 51.
[71] G. te Velde, F. M. Bickelhaupt, E. J. Baerends, C. Fonseca Guerra, S. J. A. van Gisbergen, J. G. Snijders, T. Ziegler, *J. Comput. Chem.* **2001**, *22*, 931 – 967.
[72] C. Fonseca Guerra, J. G. Snijders, G. te Velde, E. J. Baerends, *Theor. Chem. Acc.* **1998**, *99*, 391 – 403.
[73] E. J. Baerends, T. Ziegler, A. J. Atkins, J. Autschbach, D. Bashford, A. Bérces, F. M. Bickelhaupt, C. Bo, P. M. Boerrigter, L. Cavallo, D. P. Chong, D. V. Chulhai, L. Deng, R. M. Dickson, J. M. Dieterich, D. E. Ellis, M. van Faassen, L. Fan, T. H. Fischer, C. Fonseca Guerra, M. Franchini, A. Ghysels, A. Giammona, S. J. A. van Gisbergen, A. W. Götz, J. A. Groeneveld, O. V. Gritsenko, M. Grüning, S. Gusarov, F. E. Harris, P. van den Hoek, C. R. Jacob, H. Jacobsen, L. Jensen, J. W. Kaminski, G. van Kessel, F. Kootstra, A. Kovalenko, M. V. Krykunov, E. van Lenthe, D. A. McCormack, A. Michalak, M. Mitoraj, S. M. Morton, J. Neugebauer, V. P. Nicu, L. Noodleman, V. P. Osinga, S. Patchkovskii, M. Pavanello, C. A. Peeples, P. H. T. Philipsen, D. Post, C. C. Pye, W. Ravenek, J. I. Rodríguez, P. Ros, R. Rüger, P. R. T. Schipper, H. van Schoot, G. Schreckenbach, J. S. Seldenthuis, M. Seth, J. G. Snijders, M. Solà, M. Swart, D. Swerhone, G. te Velde, P. Vernooijs, L. Versluis, L. Visscher, O. Visser, F. Wang, T. A. Wesolowski, E. M. van Wezenbeek, G. Wiesenekker, S. K. Wolff, T. Woo, A. L. Yakovlev, *ADF2016*, SCM, Theoretical Chemistry, Vrije Universiteit, Amsterdam, The Netherlands, **2016**.
[74] E. van Lenthe, E. J. Baerends, J. G. Snijders, *J. Chem. Phys.* **1994**, *101*, 9783.
[75] A. D. Becke, *Phys. Rev. A* **1988**, *38*, 3098 – 3100.

Manuscript received: July 4, 2017
Accepted manuscript online: August 24, 2017
Version of record online: September 27, 2017